Electronic Supplementary File

Aqueous rechargeable Zn-ion battery: An imperishable and high-energy $Zn_2V_2O_7$ nanowire cathode through intercalation regulation†

Balaji Sambandam[a‡], Vaiyapuri Soundharrajan[a‡], Sungjin Kim[a], Muhammad H. Alfaruqi[a], Jeonggeun Jo[a], Seokhun Kim[a], Vinod Mathew[a], Yang-kook Sun[b], Jaekook Kim[a]*

[a]Department of Materials Science and Engineering, Chonnam National University, 300Yongbong-dong, Bukgu, Gwangju 500-757, South Korea; Fax: +82-62-530-1699; Tel: +82-62-530-1703

[b]Department of Energy Engineering, Hanyang University, Seoul 133-791, South Korea.

*E-mail: jaekook@chonnam.ac.kr

‡These authors contributed equally to this work.

Preparation of $Zn_2V_2O_7$ nanowires

First, solution A was prepared by dissolving $Zn(NO_3)_2 \cdot 6H_2O$ (1 mmol) in 15 ml deionized (DI) water, and solution B was prepared by adding NH_4VO_3 (2 mmol) in 15 ml hot DI water (to obtain yellow color). Second, solution B was added slowly to solution A and stirred well; the mixture was then shifted to a 50-mL Teflon-lined autoclave kept at 210 °C for 48 h and cooled naturally. The heating time was restricted to obtain a phase-pure sample. The final precipitates were filtered and washed with distilled water and ethanol, respectively, for few times, and dried under vacuum at 120 °C for 8 h to obtain phase-pure α-ZVO. The yield of the product was found to be ~95%. The as-obtained product was used directly for subsequent characterization.

Material characterization

Powder X-ray powder diffraction (PXRD, Cu Kα radiation, with λ = 1.5406 Å) measurements were conducted using a Shimadzu X-ray diffractometer. The surface texture was analyzed by field-emission scanning electron microscopy (FE-SEM, S-4700 Hitachi). The lattice fringes were analyzed using field-emission transmission electron microscopy (FE-TEM, Philips Tecnai F20 at 200 kV). Surface elemental oxidation states were examined by X-ray photoelectron spectroscopy (XPS, Thermo VG Scientific Instruments, Multilab 2000) using Al Kα as the X-ray source. The spectrometer was calibrated with respect to C 1s peak with binding energy of 284.6 eV.

Electrochemical performance

A paste containing 70, 20, and 10 wt% of the active material, Ketjen black, and Teflonized acetylene black (TAB), respectively, was pressed onto a stainless-steel mesh and vacuum drying at 120 °C for 12 h for use as the cathode. The active mass loading was found to be 3-3.5 mg. Zn metal foil and 1 M $ZnSO_4$ solution were used as the anode and electrolyte, respectively. While preparing 2032-type coin cells, a glass-fiber separator soaked in the electrolyte was pressed between the cathode and the anode under open-air conditions and aged for 12 h. Then, electrochemical discharge/charge measurements were executed using a battery tester (BTS 2004H model, NAGANO, Japan) at different current drains in the voltage space 0.4–1.4 V vs. Zn^{2+}/Zn. For cyclic voltammetry (CV) scans, a potentiostat model workstation (AUTOLAB PGSTAT302N) was used.

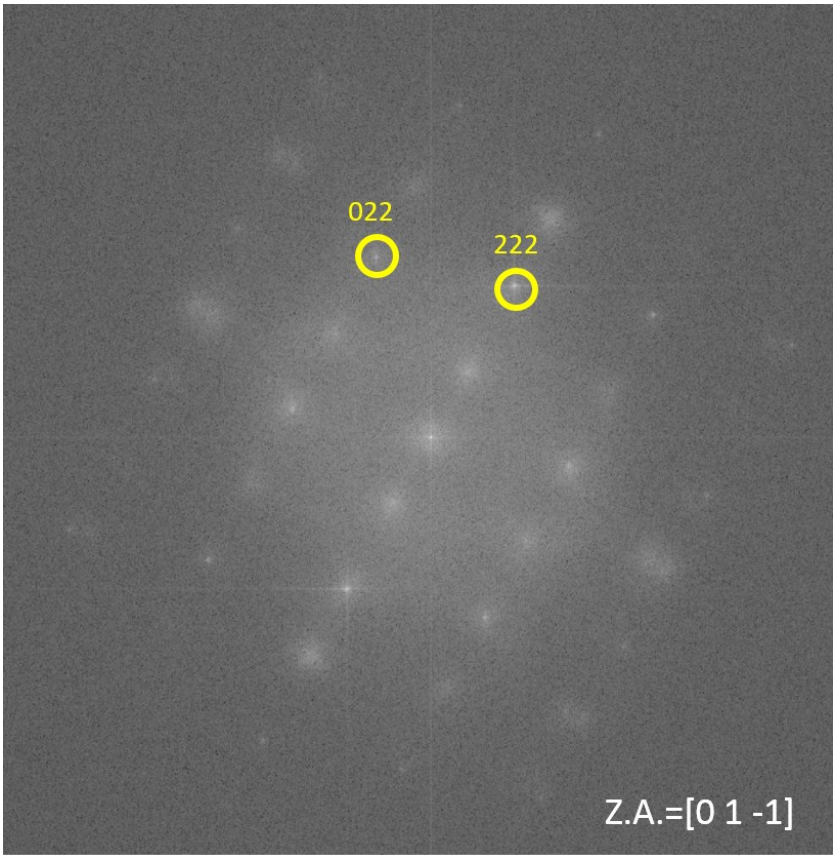

Fig. S1. FFT lattice planes image of α-$Zn_2V_2O_7$ nanowires for the corresponding TEM image found in Fig. 1(d) from the main text.

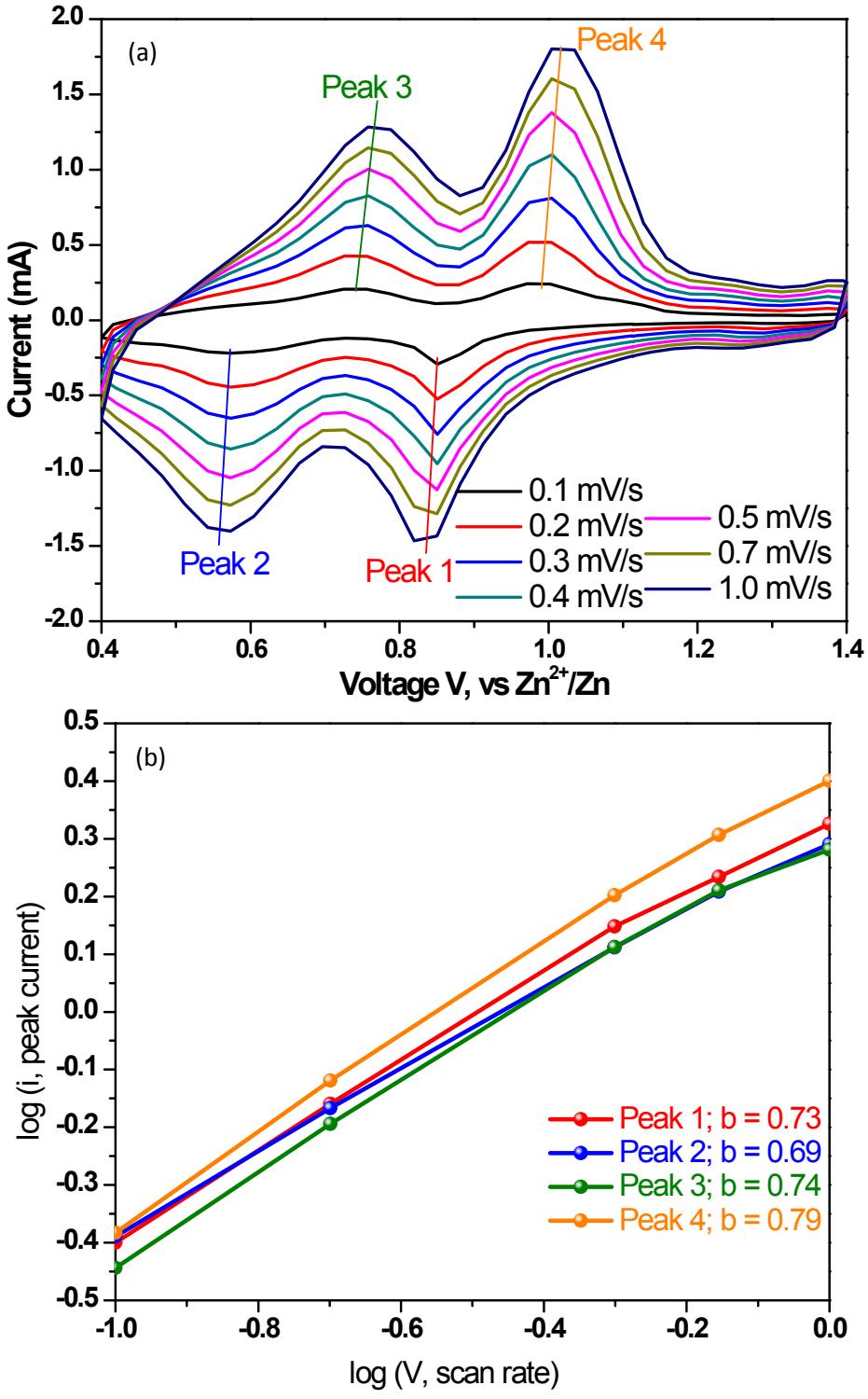

Fig. S2. (a) Multi-scan CV analysis at different scan rates from 0.1 to 1.0 mV s^{-1} to distinguish the electrochemical kinetics of α-ZVO for aqueous Zn-ion batteries, (b) log(*i*)-log(*v*) plots for specific peak currents at different scan rates to analysis the diffusion/capacity behaviors.

Based on different scan rates varies from 0.1 to 1.0 mV s^{-1} as given in Fig. S2 (top), the electrochemical kinetics process can be assumed to fit the following equation (1).[1, 2]

$$i = av^b \qquad equation(1)$$

where i and ν are the peak current (mA) and the corresponding scan rate (V s^{-1}), respectively; a and b are variable parameters in which the latter varies in the range of 0.5–1.0. For a given system, the b value of 0.5 depicts the process of diffusion-limited and the value is 1.0 indicating a capacitive process. Based on the relationship between log(i) and log(ν) for four different peaks, the b-values determined by the slopes of the four redox peaks are 0.73, 0.69, 0.74, and 0.79, inferring that the electrochemical kinetics regulation are diffusion-influenced as shown in Fig. S2 (bottom)

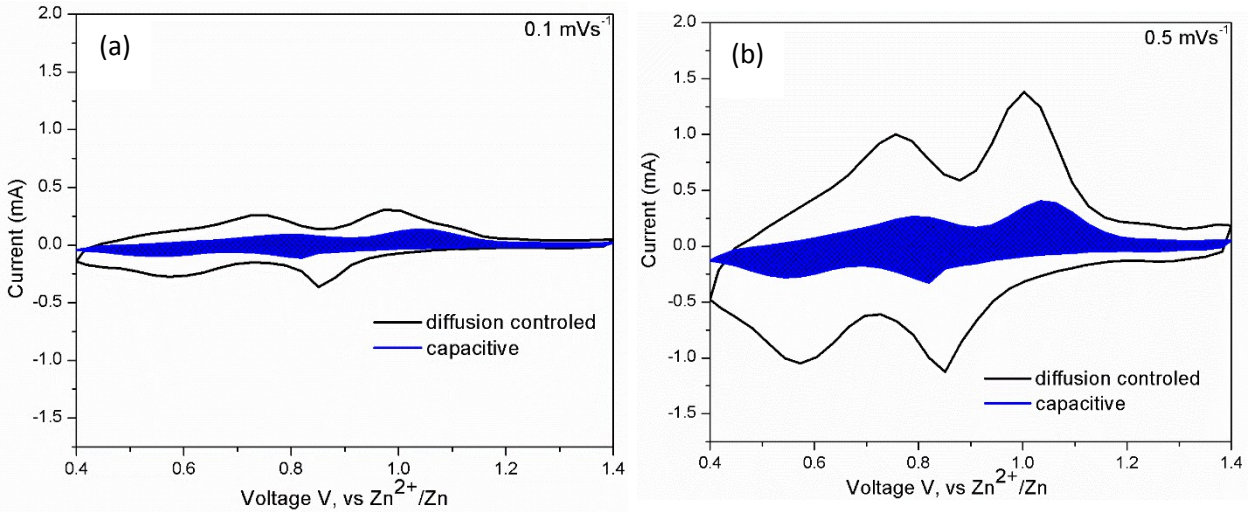

Fig. S3. The contribution ratio of the capacitive capacities and diffusion-limited capacities based on equation 2 at (a) 0.1 and (b) 0.5 mV s^{-1}.

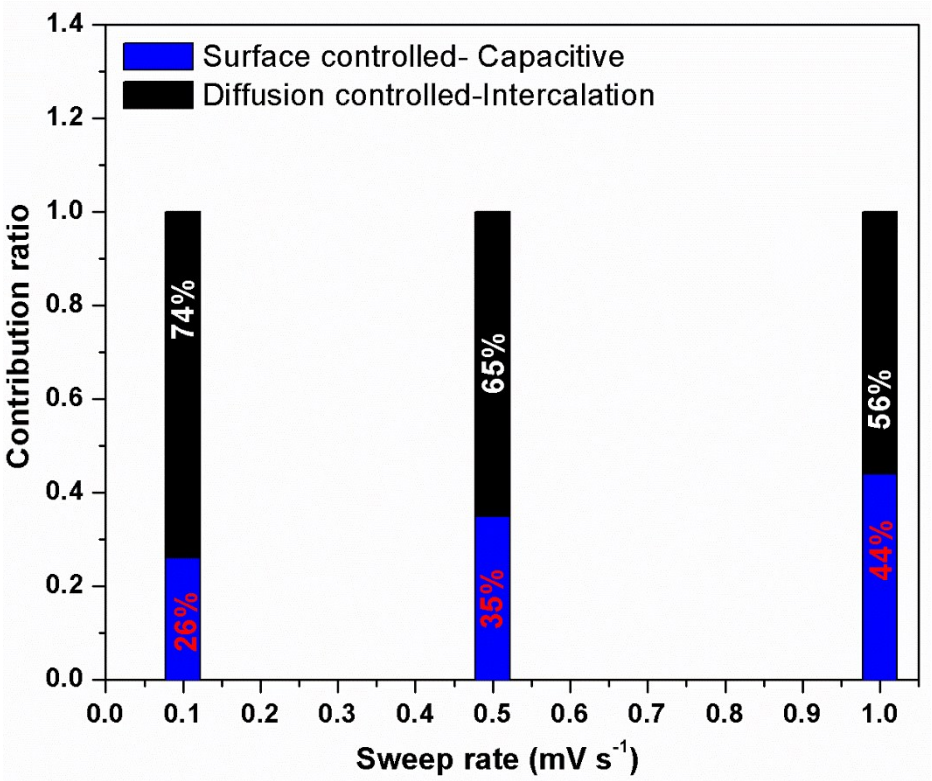

Fig. S4. Bar diagram for contribution ratio between capacitive capacities and diffusion-limited capacities for different peak currents.

From equation (1), to further analyze the combination of surface-controlled capacitive and diffusion-controlled intercalation processes, the following equation is derived.

$$i = k_1 v + k_2 v^{\frac{1}{2}} \qquad \text{equation(2)}$$

where the first and second compartments in the right side represent the capacity- and diffusion-limited redox reactions, respectively. At the scan rate of 0.5 mV s^{-1}, nearly 35% of the total current is capacity-limited (Fig. S3). Similarly, the calculated capacity- and diffusion-controlled redox values at different scan rates are calculated as given in Fig. S4. The percentage of capacitive contribution increases with increasing scan rate. However, at 1 mV s^{-1}, over 55% of the redox reaction occurs through the diffusion-controlled intercalation mechanism.

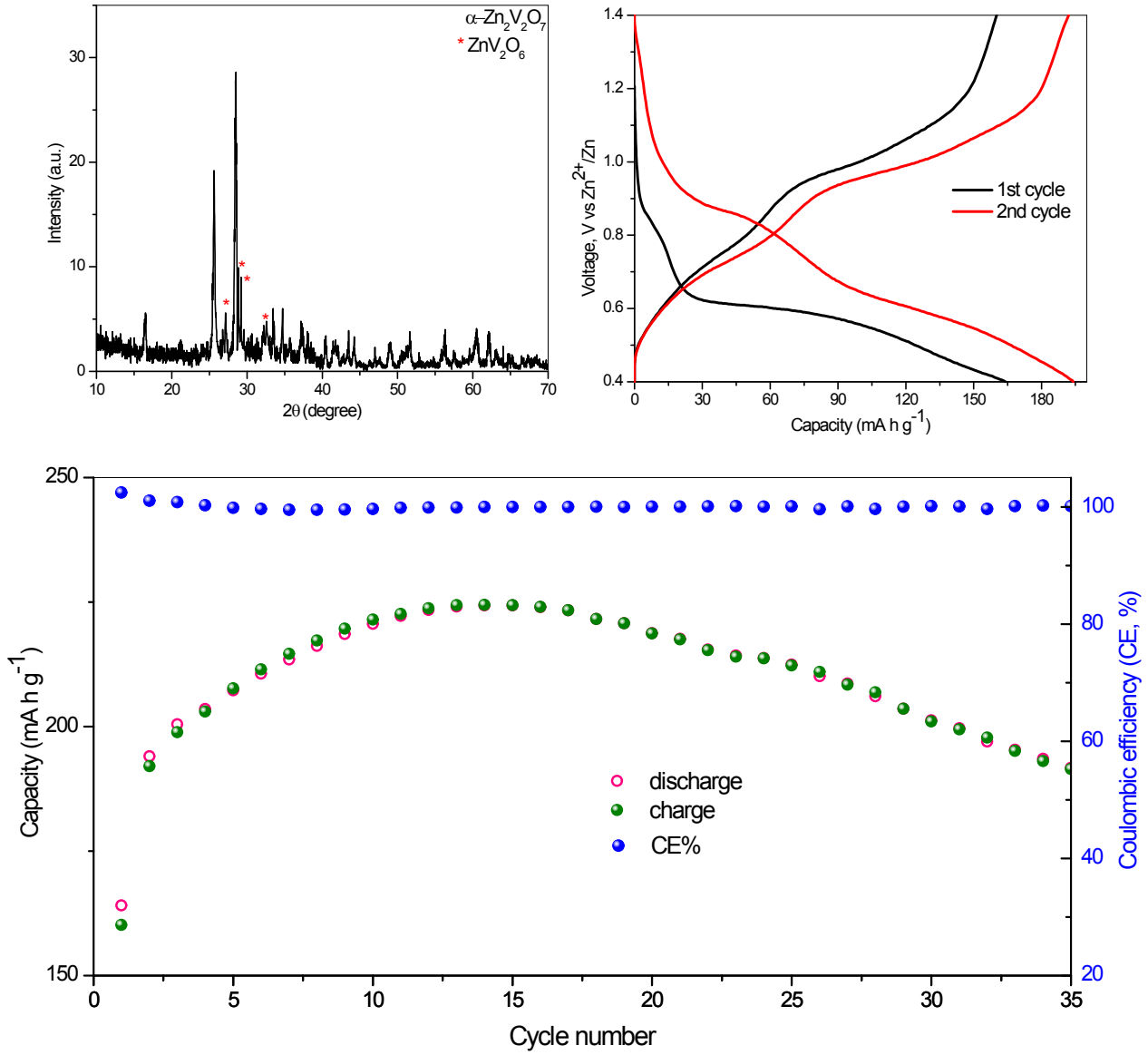

Fig. S5. (a) XRD pattern of bulk α-ZVO prepared by solid state reaction, (b) charge-discharge profiles of bulk α-ZVO under 200 mA g^{-1} of current density and (c) corresponding cyclability pattern.

The bulk α-ZVO has been prepared by solid state reaction by mixing of ZnO and V_2O_5 in 2:1 ratio. The mixture was grinded well and annealed step wise at 550 deg.cel for 45 hr in air with frequent intermediate grinding. Fig. S5a shows the XRD pattern of the α-ZVO in bulk phase with a notable impurity of ZnV_2O_6. The galavanostatic electrochemical reaction was performed under

the similar electrochemical condition used for α-ZVO nanowires electrode (Fig. S5b). An almost similar pattern was recorded on the board with respect to α-ZVO nanowires. The corresponding cyclability profile in Fig. S5s, infers the capacity fading over cycle number, after it achieved an activation.

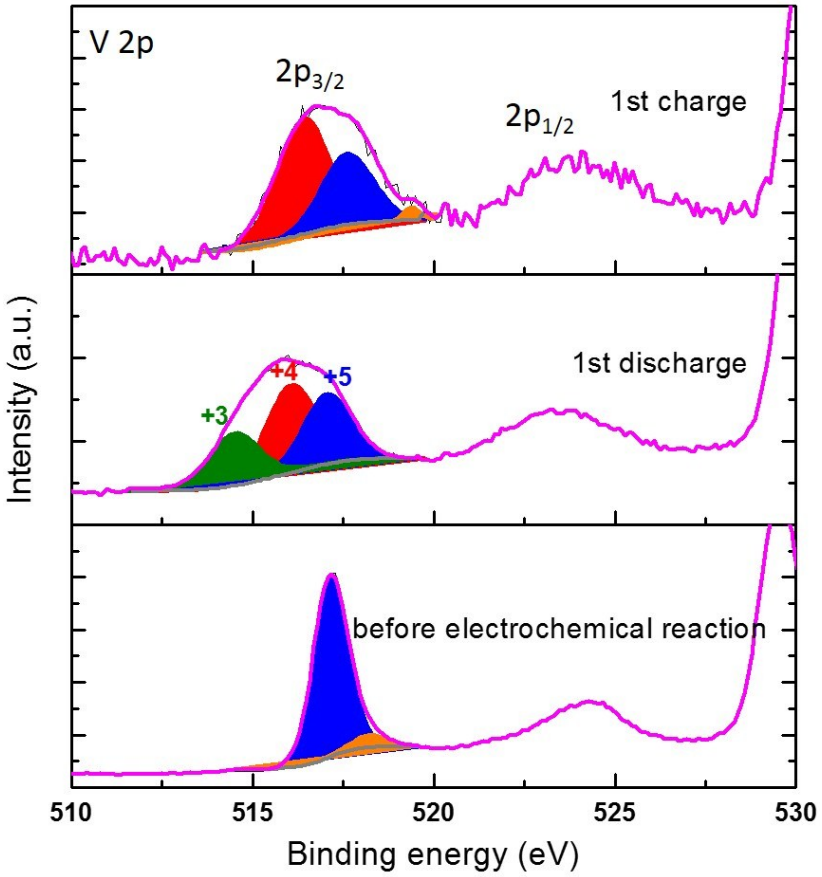

Fig. S6. Ex situ XPS study to support the electrochemical mechanism. The analysis given for V2p lines at different stages; before electrochemical reaction (bottom), at end of 1st discharge (middle) and at end of 1st charge (top).

The XPS V2p patterns for 1st discharge and charge processes after postmortem of the electrode are given in Fig. S3. The oxidation state of the vanadium is changed from +5, just before the electrochemical reaction (given in the bottom of the figure), into +3 state at the end of 1st discharge, as shown in $V2p_{3/2}$ deconvoluted profile of Fig. S3 (middle). Interestingly, the

deconvoluted profile of 1st charge (Fig. S3 top) resembles the features observed before electrochemical reaction, revealing the reversible mechanism proposed in this study. However, the observation of higher oxidation states in both cases, confirm the surface/unavoidable oxidation during the postmortem of the electrode.

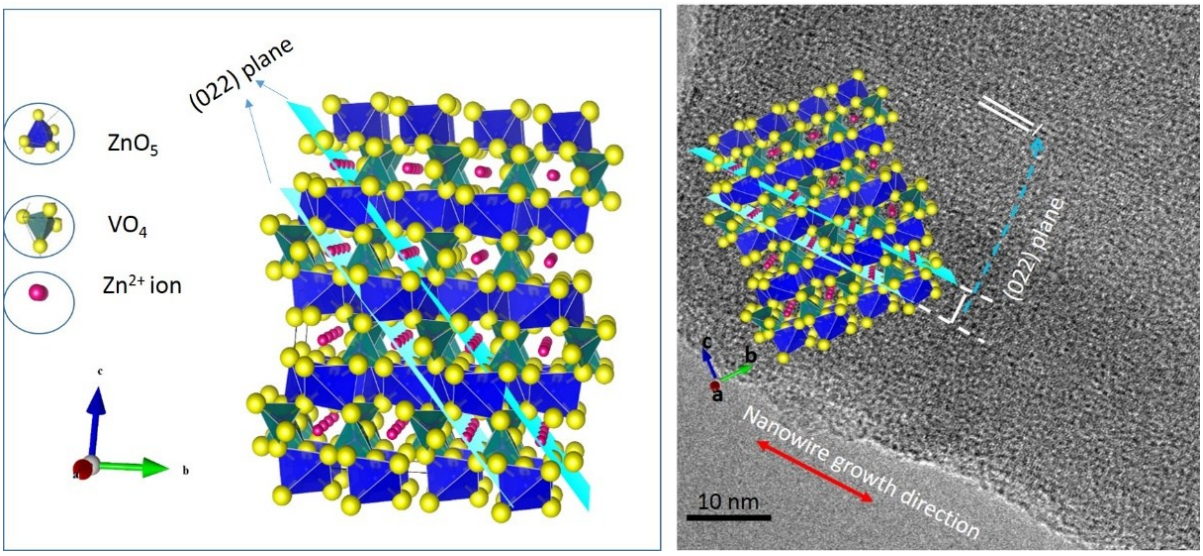

Fig. S7. (a) Crystallographic view of α-$Zn_2V_2O_7$ with notable (002) plane and (b) The migration of zinc ions into α-$Zn_2V_2O_7$ gallery is predicted by (002) lattice plane lies parallel with nanowires growth direction using VESTA software.

Specific power and specific energy calculation:

Specific power (W Kg^{-1}): I*V/2m

where I is the applied current (A), V is the cell voltage (V), m is the total active mass at cathode (g).[3, 4]

Specific energy (Wh Kg^{-1}): specific capacity * voltage (potential at which 50% of discharge capacity is reached)

References

1 L. Huang, Q. Wei, X. Xu, C. Shi, X. Liu, L. Zhou and L. Mai, *Phys. Chem. Chem. Phys*., 2017, **19**, 13696-13702.
2 Y. Wu, J. Meng, Q. Li, C. Niu, X. Wang, W. Yang, W. Li and L. Mai, *Nano Research* 2017, **10**, 2364-2376.
3 R. Thangavel, B. Moorthy, D. K. Kim and Y. S. Lee, *Adv. Energy Mater.,* 2017, **7**, 1602654.
4 M. D. Stoller and R.S. Ruoff, *Energy Environ. Sci.*, 2010, **3**, 1294-1301.